Approach Methods for Autonomous Precision Aerial Drop from a Small Unmanned Aerial Vehicle

Siri H. Mathisen * **Vegard Grindheim** * **Tor A. Johansen** *

* *Centre for Autonomous Marine Operations and Systems (NTNU AMOS), Department of Engineering Cybernetics, Norwegian University of Science and Technology (NTNU), Trondheim, Norway*

Abstract: One of the many basic operations that a fixed-wing unmanned aerial vehicle (UAV) should master autonomously is to deliver an object to a precise position. Among several possible delivery approaches, this paper chooses to focus on releasing the object from the UAV, at a carefully calculated state, and let it fall freely to the selected landing location. In such an operation, the computation of suitable release positions, velocity and attitude is essential. Due to time-varying disturbances like wind, a previously calculated release state may not be suitable once it has been reached by the aircraft. On account of these challenges, this paper suggests a dynamic calculation of the release state with respect to the wind velocity and current state of the UAV, with a sufficient re-optimization frequency. This is tested in simulation and with field tests, and compared with results from a static calculation approach.

Keywords: Control Design, Optimal Control, Aerospace, Autonomous Vehicles, Precision Drop

1. INTRODUCTION

It is useful to be able to drop objects from small unmanned aerial vehicles (UAVs). They can deliver trackers and sensors for scientific research, both off-shore and on shore, or they can be used to deliver emergency supplies or equipment. A fixed-wing UAV can be advantageous compared to a rotary wing UAV as it can usually fly further and faster, but given its nature, it is impractical to hover or land at remote locations in order to release the object. Because of limited available payload capacity and the lack of launch-and-recovery infrastructure at the target position, an airdrop of the object, sufficiently wrapped to withstand the impact, would be an effective deployment method.

In the literature, precision drop has been investigated for both manned and unmanned, civil and military aerial vehicles. When it is too impractical to deliver the payload directly to the delivery point, a mean to achieve the same precision could be to have a system to deliver the payload, while the aircraft remained in the air. This was done in Williams and Trivailo (2006), where a loitering aircraft lets a payload slide directly down to the ground along a cable. The downside to this is that a small UAV with limited payload capacity would be strained carrying a long cable. Another intuitive approach is to drop the payload directly from the body of the aircraft. A lot of research was done to develop a Joint Precision Airdrop System (JPADS), which uses steerable parachutes to guide a load to the given location, meant for military use to deliver supplies and to sustain combat power, Wright et al. (2005), Benney et al. (2005), Joshua and Eaton (2013), Tavan (2006). However, a steerable parachute would be unsuited for our purpose: Mainly it would be too expensive, as it could not be reused, and it would also be very difficult to control a very light-weight payload with a parachute in the presence of wind. Klein and Rogers (2015) have studied unguided airdrops, still using parachutes. With the aim of improving the performance of unguided drops, they present a mission planner de-

pendent on a desired impact dispersion, which finds an optimal computed air-release point (CARP) for the payload. It has also been endeavoured to improve airdrop accuracy by improving some of the parameters that lead to the error, like optimizing the parachute transition altitudes, Gerlach et al. (2016), or using models to estimate optimal release points, VanderMey et al. (2015). The simplest and most intuitive solution is to release the payload from the body of the UAV, and let it fall unguided and freely to the ground. This has been successfully tested out by McGill et al. (2011), delivering payloads to an ice berg. McGill et al. (2011) describes manually guided UAVs releasing GPS sensors without the need for high precision. They simply released the payload when they were certain that the ice berg was underneath.

This paper considers the control of autonomous high-precision drop of a generic object from a fixed-wing UAV. The UAV should calculate its release state onboard, to ensure autonomous operation with as high precision on the impact point as possible. It is necessary not only to calculate the correct point of release given the known wind, but also to approach this point in a correct state. The approaching speed and attitude of the UAV will decide the ballistic path of the released payload, and it is essential to take the wind into consideration. Therefore, the approach decides which release state will be the appropriate one to use in the given situation. To combine airspeed and ground velocity measurements, a wind velocity estimator is used.

In this paper, a comparison of the accuracy of three different approach methods is performed, one static and two dynamic approaches. We want to study dynamic planning of the release point and its approach to achieve a high precision for the released payload with good robustness for shifting wind, and we want to find out when it is advisable to change the path to our release point. Preliminary results can be read in Mathisen (2014) and Grindheim (2015).

2. COMPUTED AIR-RELEASE POINT

Given the target location, a set of feasible release points can be calculated, depending on incoming velocity, wind velocity and height over target. The choice of release point then decides how to approach that position. Given the drag force equation $F_D = \frac{1}{2}C_D A \rho V_a^2$ (Beard and McLain, 2012), where C_D is the drag coefficient, ρ is the density of the fluid (air), A is the projected area of the body relative to its movement and V_a is the speed of the body relative to the fluid. Newton's 2nd law, assuming only drag force and gravity acting on the falling body, is:

$$m \begin{bmatrix} \dot{v}_x \\ \dot{v}_y \\ \dot{v}_z \end{bmatrix} = -m \begin{bmatrix} 0 \\ 0 \\ g \end{bmatrix} + \begin{bmatrix} F_{Dx} \\ F_{Dy} \\ F_{Dz} \end{bmatrix}, \qquad (1)$$

where m is the mass of the body, g is the gravitational acceleration constant and the decomposed drag forces are:

$$\begin{aligned} F_{Dx} &= -\frac{1}{2}C_D A \rho V_a^2 \frac{u_r}{V_a}, \\ F_{Dy} &= -\frac{1}{2}C_D A \rho V_a^2 \frac{v_r}{V_a}, \\ F_{Dy} &= -\frac{1}{2}C_D A \rho V_a^2 \frac{w_r}{V_a}, \end{aligned} \qquad (2)$$

where the drag force is transformed from the wind frame to the body frame of the object. The ballistic equations are given by:

$$\dot{\mathbf{x}} = \begin{bmatrix} v_x \\ v_y \\ v_z \\ -\frac{1}{2m}C_D A \rho V_a^2 \frac{u_r}{V_a} \\ -\frac{1}{2m}C_D A \rho V_a^2 \frac{v_r}{V_a} \\ -g - \frac{1}{2m}C_D A \rho V_a^2 \frac{w_r}{V_a} \end{bmatrix} \qquad (3)$$

where the states $\mathbf{x} = [x \; y \; z \; v_x \; v_y \; v_z]^\top$ is a vector of North-East-Down positions and linear velocities and u_r, v_r and w_r are the body velocities relative to the fluid. The displacement between the CARP and the target is computed numerically by applying Euler's method to Eq. 3 using wind velocity estimates. The problem is further delimited by assuming the UAV has constant, known velocity at the release point and zero vertical velocity, that the release altitude is constant and known, and that the object is released while the UAV is flying against the wind. This delimitation gives a circle of possible CARPs at the given height above the landing position. When a constant wind is included, the center of the circle moves, see Fig. 1.

3. ON-BOARD PATH COMPUTATION

Once the CARP is calculated, the on-board computer calculates a path from the current position using Dubins-path theory, Beard and McLain (2012): At the same altitude, a point p is chosen a distance d away from the CARP in the wind direction. Drawing a line through the CARP and p, a circle with radius r can be constructed tangential to the line in p. The circle is chosen such that the trajectory along a part of the circle, ending
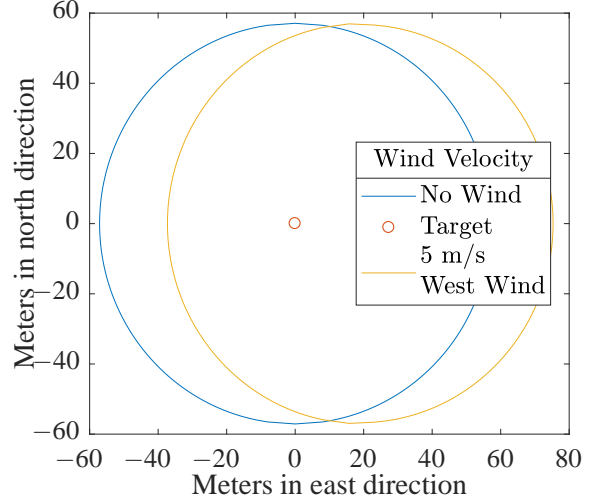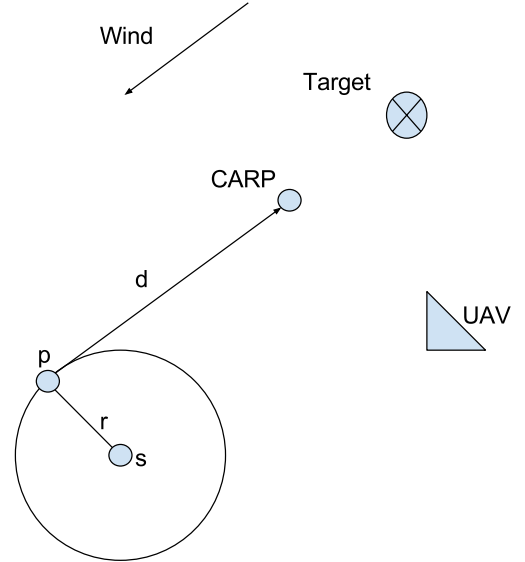

Fig. 1. Possible CARPS with and without wind

Fig. 2. Initial approach towards CARP: The UAV makes a turn to approach the CARP against the wind. When p is reached, the UAV can either fly directly to that point or continuously update CARP.

in p and directly thereafter continuing along the line towards the CARP, will be clockwise. The UAV will approach this circle from whichever direction is closer, and fall into a clockwise arc that ends in point p and then continues straight towards the CARP.

3.1 Static CARP

In the static guidance method, the CARP is calculated again once at point p, see Fig. 2. The calculation considers not only wind, but also the UAV's present velocity and position. This approach is shown in Fig. 3, where the set of all possible CARPs are denoted feasible air-release points (FARPs). n possible FARPs are calculated, accounting for the estimated wind velocity at the moment. A minimization using a weighted sum of the difference in velocity and distance between each FARP and the UAV is performed, and the optimal FARP is then set as the new CARP. Once this CARP has been calculated, changes
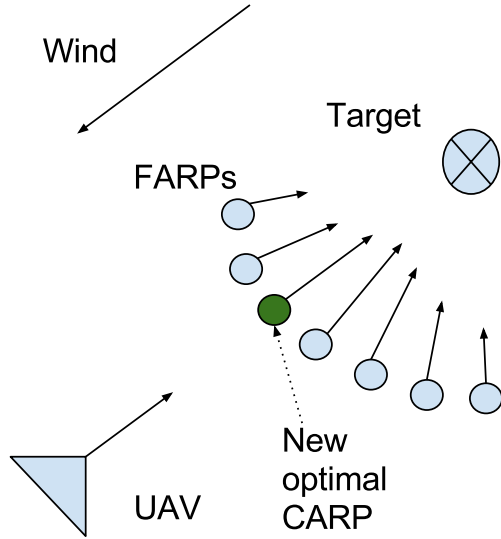
Fig. 3. Selection of optimal CARP

in wind or other disturbances will not be considered any more. The UAV continues until it has reached CARP, releases the object and continues with its mission.

3.2 Dynamic CARP

In the dynamic guidance method, the CARP is calculated at point p, just as in the static guidance method, but then the CARP is recalculated at regular intervals, using the same procedure as previously described. Once a new CARP has been calculated, the UAV is guided along a trajectory to this point with desired velocity.

3.3 Conditional Re-optimization

The conditional re-optimization works just like the dynamic-CARP guidance method described in the previous section, but it will only track the new CARP if the predicted tracking error with the old CARP is larger than a given constant. So instead of resetting the CARP for the UAV with a fixed time interval, this method changes the optimal CARP whenever necessary.

4. UNMANNED AERIAL SYSTEM ARCHITECTURE

The test bed used for the flight tests is a X8 flying wing from Skywalker Technology and Co. with a maximum take-off mass of 4.5 kg. It uses a Pixhawk autopilot from ArduPilot using 5 GHz Radio Communication equipment from Ubiquity, and an external ublox NEO6 GPS. The payload computer is a Beagle Bone Black carrying a AM335x 1GHz ARM Cortex-A8 processor with GLUED Linux based operating system. The object to be released is attached to the UAV using an EFLA405 Servoless Payload Release, controlled by a PWM signal.

4.1 The LSTS Toolchain

To facilitate the communication between the user, the autopilot and the payload computer program, the LSTS toolchain is implemented, LSTS (2015). This is software that facilitates operation with unmanned vehicles and includes the unified navigation environment (DUNE), the inter-module communication

protocol (IMC), the operating system distribution GLUED and the command and control center Neptus. For more information about the LSTS Toolchain, see e.g. Pinto et al. (2012), Pinto et al. (2013). For a more detailed description of the architecture for the unmanned aerial system, see Zolich et al. (2015). The UAV is guided by the autopilot with a Line of Sight and Sliding Mode controller described by Fortuna and Fossen (2015).

4.2 Wind Estimator

To be able to deliver the object to a precise location, it is critical to have correct information about the wind velocity. In this paper we will use the UAV's position and velocity delivered by the Pixhawk, and in this section concentrate on an estimate for the wind velocity. The structure of the estimator used in this paper is described in detail in Johansen et al. (2015). Based on a Kalman Filter, an estimate for the mean wind velocity in three dimensions at the UAVs body is found. The required sensors are a Global Navigation Satellite System (GNSS) to provide velocity over ground measurements, an Inertial Measurement Unit (IMU) to provide attitude measurements, and a pitot-static tube to provide measurements of the airspeed. To get convergence of the estimator error, the attitude of the aircraft cannot be constant. This means that a flight in a circle would enable the estimations of wind velocity, which makes this wind estimator well suited for the flight pattern described in this paper. The wind velocity estimator is implemented as a task in DUNE, delivering the wind estimate as an IMC message to the payload system. The measurements come from the autopilot's IMU and pitot-static tube and from an external GPS.

5. SOFTWARE IN THE LOOP SIMULATIONS

The system was tested using Software in the Loop (SITL) to analyse the performance of the different CARP calculation methods. The tests were carried out using a simulator for the Pixhawk, MAVProxy Ground Control Software with the JSBSim physical environment and flight dynamics simulator, and Neptus from LSTS to visualize the simulations. The wind turbulence model used in JSBSim for the simulations was is Milspec (FlightGear (2015)), using a Dryden turbulence spectrum model. The intensity of the turbulence can be set as a parameter for the simulations, where 0 is calm and 1.0 is severe. Prerequisites to the tests are a target around 500 meters away from the UAV, which loiters over the sea.

5.1 Test Cases

A target is set manually from Neptus and sent to the payload program on the simulated UAV. This target is kept at the same altitude as the UAVs current position, at a safe height above the ground. This program calculates the CARP, as well as a point p that is 200 m away from the the release point and a circle tangent to p around the point s, see Fig. 2. The condition for release of the payload is given in Eq. 4:

$$(d_k < D_{MAX} \; AND \; d_k > d_{k-1}) \; OR \; (d_k < 1.0) \tag{4}$$

at time step k. Once the object has been dropped from the UAV, the SITL calculates a hitpoint on the ground for the payload: With simulated turbulence following the Dryden model and following the ballistic path from Eq. 3, each drop has a simulated hit to the ground for the payload. The characteristic parameters for the simulations are presented in Table 1.

5.2 Results

The results from the simulations are shown in Figs. 4 and 5. Figs. 6 and 7 show the implemented wind estimator's performance compared to the autopilot's wind estimates, with low and strong turbulence respectively. The results are discussed in Section 7.

6. FLIGHT TESTS

The system performed drop tests in March 2017 on Agdenes Airport, Breivika. Due to the surroundings on this airport, the distance d between the CARP and the last point of the loiter circle was reduced from 200 m to 100 m (see Fig. 2), the frequency of re-optimizations for the two dynamic methods for CARP calculations was decreased to 2.5 Hz and the acceptance radius for CARP error was increased to 10 meters. The UAV was flying on an altitude of 80 metres, with an airspeed of 18 m/s. The wind was measured to be between 2 m/s and 4 m/s coming from south and south-east (see Fig. 8 for the wind data). Three drop tests were performed with each guidance method, in total nine drop tests. The resulting target errors and measured CARP errors are shown in Table 2. The data from the wind estimator compared to the wind data from the autopilot is shown in Fig. 8. The object that was dropped was shaped similar to a hockey puck with mass of 312 g. The parameters used in the program during the flight test were an area perpendicular to the wind of 64 cm^2, incorrectly a mass of 104 g and C_D of 0.39.

7. DISCUSSION

7.1 Wind Estimator

Figs. 6 and 7 show simulated wind data with high and low turbulence. There is by the author no known way of reading

Table 1. Characteristic parameters used in the SITL simulations.

Parameter	Value
Optimization points	60
Optimization Sector of circle	1
Optimization weighing parameter for velocity	1
Optimization weighing parameter for distance	5
UAV air speed	18 m/s
Wind Estimate Frequency	10 Hz
Autopilot data Frequency	25 Hz
Optimization Frequency	5 Hz
Simulation step size	0.001 s
Altitude	80.0 m
D_{MAX}	10 m
Maximum CARP error for conditional re-calculation	0.5 m

Table 2. Drop Error from Flight Test in Breivika

Guidance Method	CARP Error	Measured hit error	Simulated hit error
Static CARP	13.25 m	14.7 m	17.47 m
Static CARP	2.03 m	4.5 m	5.42 m
Static CARP	6.19 m	3.6 m	3.9 m
Dynamic CARP	2.18 m	4.6 m	0.68 m
Dynamic CARP	2.45 m	4.0 m	1.08 m
Dynamic CARP	5.12 m	1.0 m	6.66 m
Conditional Re-optimizing	1.53 m	6.2 m	2.8 m
Conditional Re-optimizing	4.14 m	12.4 m	4.12 m
Conditional Re-optimizing	5.65 m	4.9 m	9.44 m

the exact wind produced by JSBSim, which is the reason for using only the steady wind for reference. As the turbulence wind velocities are not shown in the plots, it must only be assumed that when the autopilot and wind estimator deviate more from the steady wind, this is because of turbulence. Comparing the two plots, it seems like the turbulence does not affect the difference between the autopilot's wind velocity estimates and the implemented wind estimator's estimates. It can then be assumed that the error caused by turbulence is no greater at the implemented wind velocity estimator than at the autopilot's. Throughout the simulation, the estimator's outputs are closer to the steady state wind than the autopilot's estimates for both wind components. Without knowing the turbulence exactly, it is difficult to say which is the more accurate.

The wind data from one flight test is shown in Fig. 8. The wind velocity of the implemented wind estimator and the autopilot estimates have an offset, and the implemented wind estimator appears to have a larger amplitude than the autopilot. As in the simulations, there is no way of telling which estimates are the more correct ones. The wind data appears to be oscillating, which might indicate a wind that changes slowly with time, and a UAV that flies in circles. The implemented wind estimator's signal does not appear to contain more noise than the autopilot's. The difference between the estimator and the autopilot varies, however not dramatically.

7.2 SITL

Figs. 4 and 5 show the target error and CARP error in multiple simulations for various wind strengths and guidance methods. The CARP error means the geographical difference between where the payload was actually commanded released from the UAV, and the optimal CARP given the present wind and UAV state. Fig. 5 shows how well the UAV meet the control objective, and is a measure of the performance of the Ardupilot and the controller used in DUNE. The static method performs slightly worse than the two dynamic approaches, and the conditional re-optimization is a bit better than the regular one. This could indicate that the frequency of recalculating the CARP was well tuned.

The standard deviation of the CARP error is approximately the same for all methods, though slightly larger for the conditional re-optimization. The mean value of the CARP error increases with increased wind for the static approach, but it is approximately the same for the dynamic approaches. The standard deviation for the target error increases with increased wind, as is natural as the varying wind has more influence on the hit position when increased in size. Here, the dynamic approaches are more accurate than the static. The offset of a hit coming from a perfect release point could be changed by adjusting the drop time, and that was accounted for in the simulations. The maximum drop error D_{MAX} from Eq. 4 was quite high, as the intention of the experiment was to compare the accuracy of the different methods. A higher accuracy could be achieved by setting the maximum drop error much lower, and measure the frequency of re-tries.
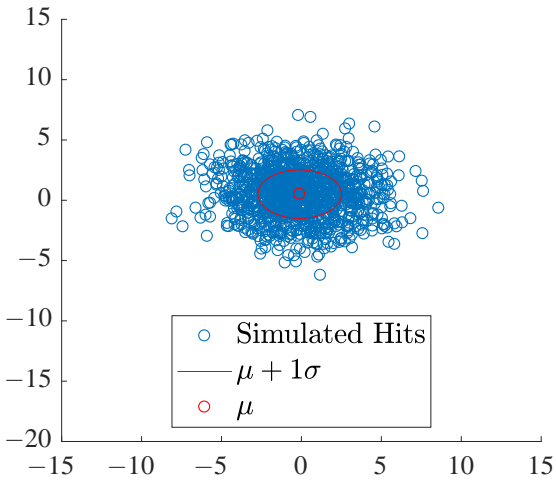
7.3 Flight Tests

Overall, the results from the flight tests were good. However, with only nine drops, and only three with each method, it is
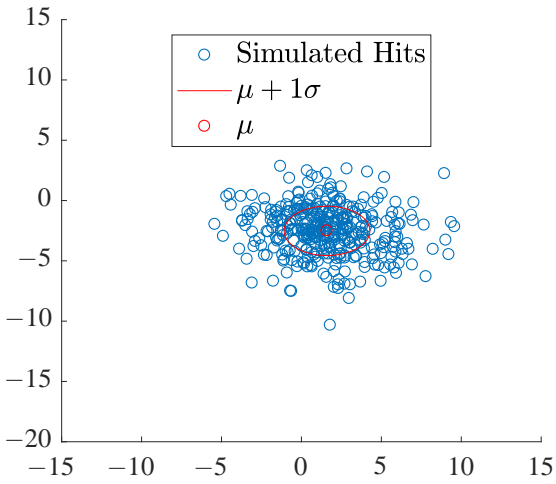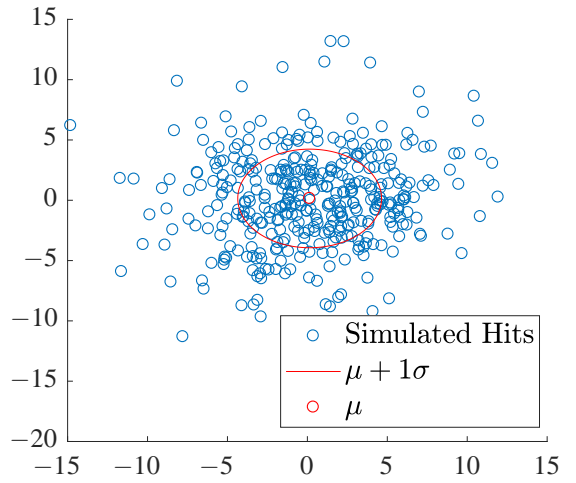
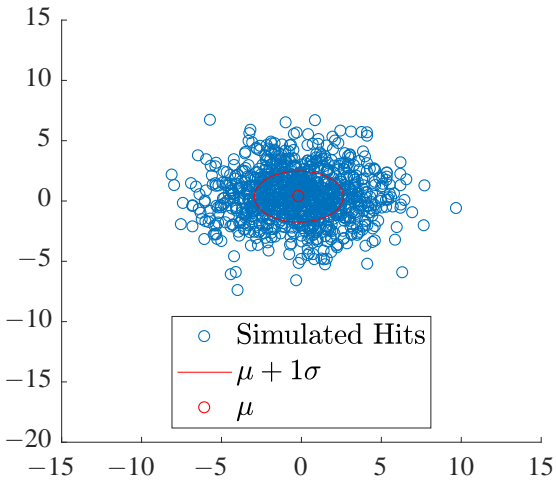(a) Static CARP, wind = 4 m/s: $\mu_x = 1.60m$, $\mu_y = -2.51m$, $\sigma_x = 2.68m$, $\sigma_y = 2.05m$
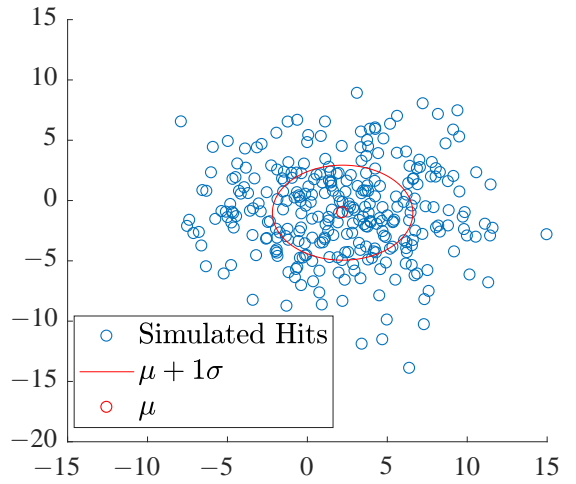
(b) Static CARP, wind = 8 m/s: $\mu_x = 2.21m$, $\mu_y = -1.01m$, $\sigma_x = 4.39m$, $\sigma_y = 3.94m$
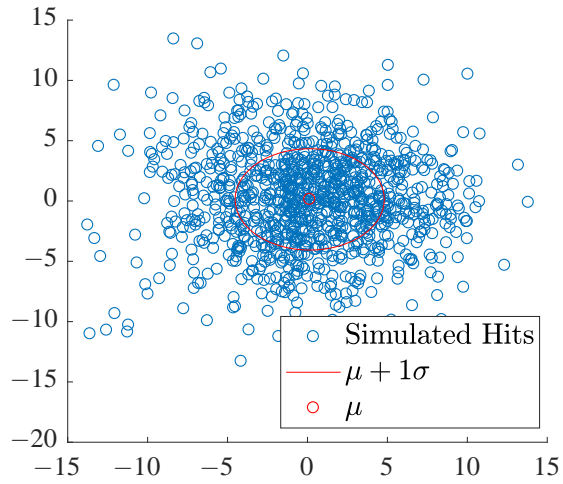
(c) Dynamic CARP, wind = 4 m/s: $\mu_x = -0.11m$, $\mu_y = 0.51m$, $\sigma_x = 2.61m$, $\sigma_y = 2.01m$

(d) Dynamic CARP, wind = 8 m/s: $\mu_x = 0.14m$, $\mu_y = 0.15m$, $\sigma_x = 4.50m$, $\sigma_y = 4.09m$
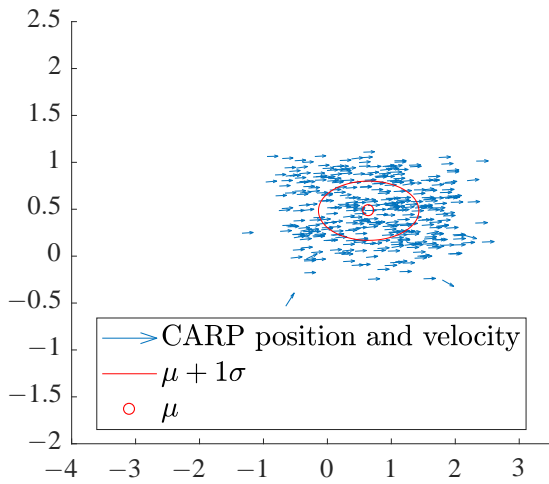
(e) Conditional re-optimization, wind = 4 m/s: $\mu_x = -0.16m$, $\mu_y = 0.36m$, $\sigma_x = 2.78m$, $\sigma_y = 2.12m$

(f) Conditional re-optimization, wind = 8 m/s: $\mu_x = -0.14m$, $\mu_y = 0.13m$, $\sigma_x = 4.66m$, $\sigma_y = 4.20m$

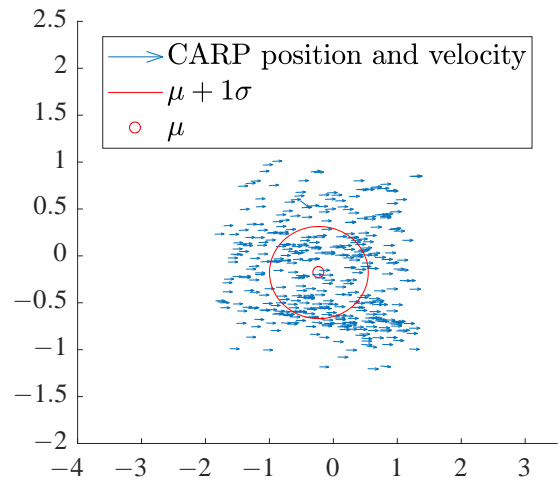Fig. 4. Simulated hits with low turbulence. Origo equals target.

(a) Static CARP, wind = 4 m/s: $\mu_x = 0.65m$, $\mu_y = 0.48m$, $\sigma_x = 0.79m$, $\sigma_y = 0.32m$
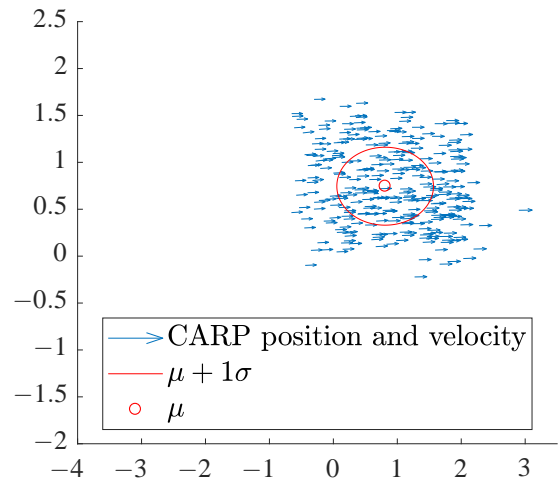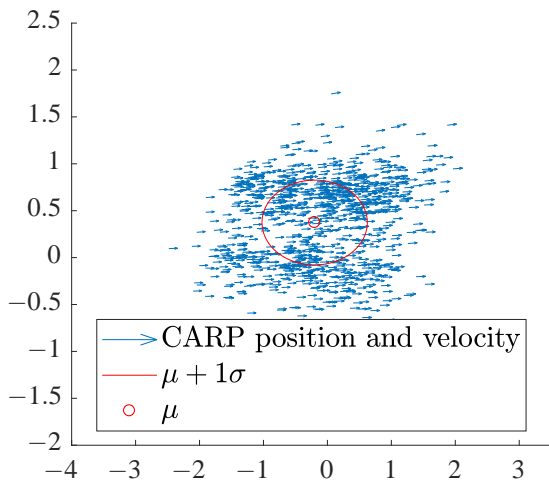
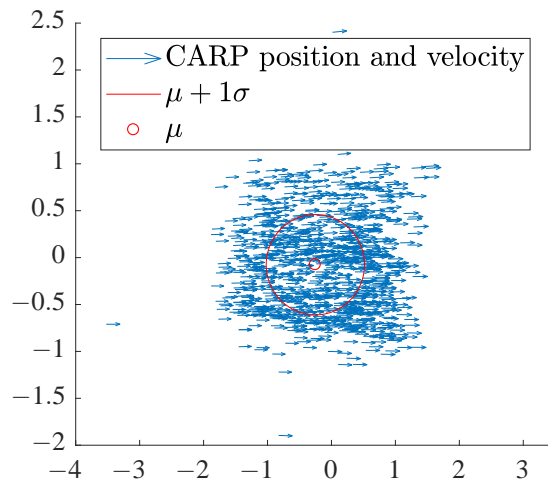(b) Static CARP, wind = 8 m/s: $\mu_x = 0.81m$, $\mu_y = 0.75m$, $\sigma_x = 0.76m$, $\sigma_y = 0.42m$
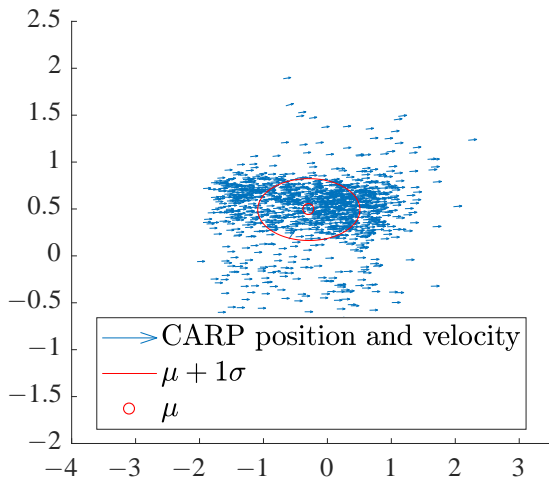
(c) Dynamic CARP, wind = 4 m/s: $\mu_x = -0.29m$, $\mu_y = 0.49m$, $\sigma_x = 0.80m$, $\sigma_y = 0.33m$

(d) Dynamic CARP, wind = 8 m/s: $\mu_x = -0.22m$, $\mu_y = -0.17m$, $\sigma_x = 0.76m$, $\sigma_y = 0.54m$

(e) Conditional re-optimization, wind = 4 m/s: $\mu_x = -0.20m$, $\mu_y = 0.37m$, $\sigma_x = 0.82m$, $\sigma_y = 0.45m$

(f) Conditional re-optimization, wind = 8 m/s: $\mu_x = -0.25m$, $\mu_y = -0.08m$, $\sigma_x = 0.77m$, $\sigma_y = 0.54m$

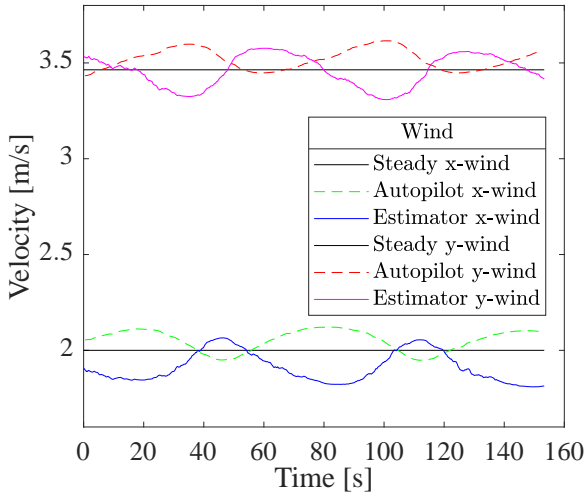Fig. 5. Simulated release positions and directions with low turbulence. Origo is the optimal CARP.

Fig. 6. The Autopilot's estimates of the wind compared to the implemented estimator's while loitering, using the constant steady wind as reference. Simulations with low turbulence intensity.

Fig. 8. The Autopilot's estimates of the wind in a solid line, compared to the implemented estimator's in dotted line. North wind in red, east wind in blue and down wind in magenta. Measured while performing a drop.
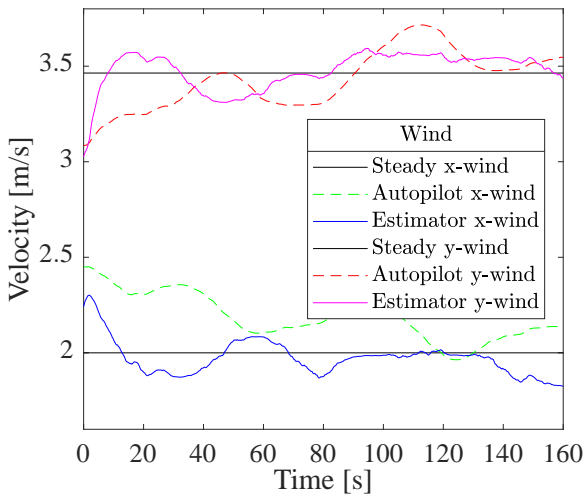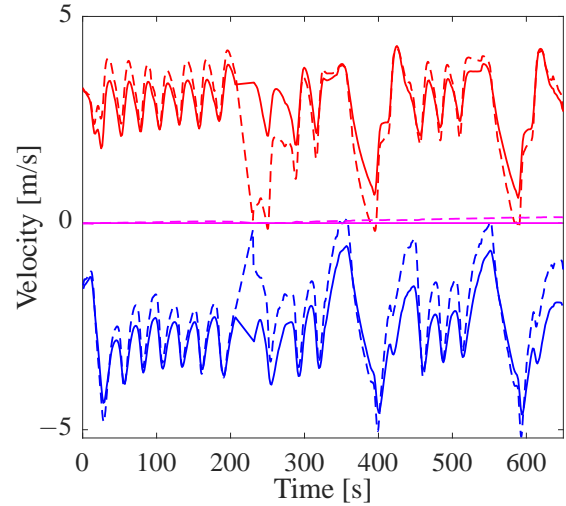

Fig. 7. The Autopilot's estimates of the wind compared to the estimator's while loitering, using the constant steady wind as reference. Simulations with high turbulence intensity.
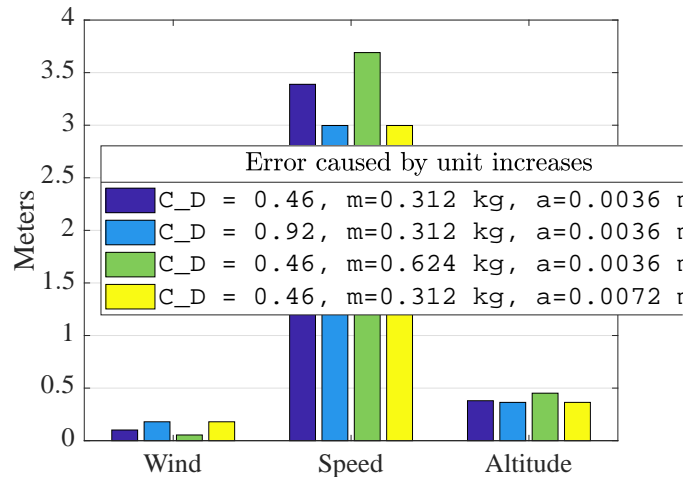

Fig. 9. Target error due to unit increase in wind, speed and height respectively. Original drop from 80 meters altitude, at 18 m/s and wind equal to 4 m/s.

difficult to compare the methods and say anything with statistical significance about the results. A sensitivity analysis of a unit change in altitude, wind and speed of the UAV showed that from a drop height of 80 meters, the speed affected the landing position of the dropped object most (see Fig. 9). The error was also gravely affected by the payload mass, area perpendicular to the wind and drag coefficient of the dropped object. However, the accuracy of the wind, ground speed and altitude estimates and measurements is not the same: The GPS in use has a velocity accuracy of 0.1 m/s and a horizontal position accuracy of 2.5 m, www.u-blox.com (2017). The altitude accuracy is normally approximately 1.5 times the horizontal accuracy, www.gps.gov (2008). As a consequence, the speed component of the error is approximately 0.3 meters, while the height component is approximately 3.5 meters. Another error source would be the simplifications of the ballistic equations for the drop, Eq. 3, which omit lift and do not consider the spin of the falling object, and the parameters for the object that was dropped. The

parameters used in the flight test were an area perpendicular to the wind of 64 cm^2, a mass of 104 g and C_D of 0.39. The material used in the dropped object was denser than the one of the initial tests, and the error of the mass of the dropped object was therefore discovered after the experiment. After observing how the dropped object hit the snow on the ground, area perpendicular to the wind while dropped is assumed to be the side of the object, and calculated to be 38 cm^2. According to Haché (2002), the drag coefficient of a hockey puck is $C_D = 0.46$ for the side and $C_D = 0.56$ for the top, therefore assuming a drag coefficient error of approximately 0.07. The estimated error composed by these sources would be approximately 10.8 meters. The mentioned errors can be accounted for by use of a real time kinematic (RTK) navigation system, and by using correct parameters for the dropped object. What is not so easily accounted for is the error introduced by the time it takes to drop the object from the UAV. In the calculations, the time from the

signal is sent to the object is falling freely is set to 0.4 s. This has been tested in the lab, but not in the air, with a moving UAV.

ACKNOWLEDGEMENTS

REFERENCES

Beard, R.W. and McLain, T.W. (2012). *Small unmanned aircraft: Theory and practice*. Princeton University Press.

Benney, R., Barber, J., McGrath, J., McHugh, J., Noetscher, G., and Tavan, S. (2005). The new military applications of precision airdrop systems. In *Infotech at Aerospace*.

FlightGear (2015). JSBSim Atmosphere. URL wiki.flightgear.org JSBSim_Atmosphere. .

Fortuna, J. and Fossen, T.I. (2015). Cascaded line-of-sight path-following and sliding mode controllers for fixed-wing uavs. In *Proc. of the 2015 IEEE Multi-Conference on Systems and Control*. 2015 IEEE Multi-Conference on Systems and Control.

Gerlach, A.R., Manyam, S.G., and Doman, D.B. (2016). Precision airdrop transition altitude optimization via the one-in-a-set traveling salesman problem. In *American Control Conference (ACC)*.

Grindheim, V. (2015). *Accurate Drop of GPS Beacon Using the X8 Fixed-Wing UAV*. Master's thesis, Norwegian University of Science and Technology, Department of Engineering Cybernetics.

Haché, A. (2002). *The Physics of Hockey*. Johns Hopkins University Press.

Johansen, T.A., Cristofaro, A., Sorensen, K.L., Hansen, J.M., and Fossen, T.I. (2015). On estimation of wind velocity, angle-of-attack and sideslip angle of small uavs using standard sensors. In *International Conference on Unmanned Aircraft Systems*.

Joshua, M. and Eaton, A.N. (2013). Point of impact: Delivering mission essential supplies to the warfighter through the joint precision airdrop system. In *Systems Conference (SysCon)*.

Klein, B. and Rogers, J.D. (2015). A probabilistic approach to unguided airdrop. In *Aerodynamic Decelerator Systems Technology Conferences*.

LSTS (2015). LSTS Toolchain. URL http://lsts.fe.up.pt/toolchain. .

Mathisen, S.H. (2014). *High Precision Deployment of Wireless Sensors from Unmanned Aerial Vehicles*. Master's thesis, Norwegian University of Science and Technology, Faculty of Information Technology, Mathematics and Electrical Engineering, Department of Engineering Cybernetics.

McGill, P., Reisenbichler, K., Etchemendy, S., Dawe, T., and Hobson, B. (2011). Aerial surveys and tagging of free-drifting icebergs using an unmanned aerial vehicle (uav). *Deep Sea Research Part II: Topical Studies in Oceanography*, 58.

Pinto, J., Calado, P., Braga, J., Dias, P., Martins, R., Marques, E., and Sousa, J. (2012). Implementation of a control architecture for networked vehicle systems. In *3rd IFAC Workshop on Navigation, Guidance and Control of Underwater Vehicles*.

Pinto, J., Dias, P.S., Martins, R., Fortuna, J., Marques, E., and Sousa, J. (2013). The lsts toolchain for networked vehicle systems. In *OCEANS - Bergen, 2013 MTS/IEEE*.

Tavan, S. (2006). Status and context of high altitude precision aerial delivery systems. In *AIAA Guidance, Navigation, and Control Conference and Exhibit Keystone*.

VanderMey, J.T., Doman, D.B., and Gerlach, A.R. (2015). Release point determination and dispersion reduction for ballistic airdrops. *Journal of Guidance, Control, and Dynamics*, 38(11).

Williams, P. and Trivailo, P. (2006). Cable-supported sliding payload deployment from a circling fixed-wing aircraft. *Journal of Aircraft*, 43(5), 1567–1570.

Wright, R., Benney, R., and McHugh, J. (2005). Precision airdrop system. In *18th AIAA Aerodynamic Decelerator Systems Technology Conference and Seminar*.

www.gps.gov (2008). Global positioning system standard positioning service performance standard. .

www.u-blox.com (2017). Neo-6 u-blox 6 GPS Modules Data Sheet. .

Zolich, A.P., Johansen, T.A., Cisek, K.P., and Klausen, K. (2015). Unmanned aerial system architecture for maritime missions. design and hardware description. In *Workshop on Research, Education and Development of Unmanned Aerial Systems (RED_UAS)*.